

MODELLING HEAT LOSS EFFECTS IN THE LES OF A LEAN SWIRL-STABILISED FLAME CLOSE TO BLOW-OFF

James C. Massey*, Zhi X. Chen* and Nedunchezian Swaminathan*
jcm97@cam.ac.uk

*Department of Engineering, University of Cambridge, Trumpington Street,
Cambridge CB2 1PZ, United Kingdom

Abstract

The flame in a model gas turbine combustor close to blow-off is studied using large eddy simulation with the objective of investigating the sensitivity of including different heat loss effects within the modelling. A presumed joint probability density function approach based on the mixture fraction and progress variable with unstrained flamelets is used. The normalised enthalpy is included in the probability density function to account for heat loss within the flame. Two simulations are presented with fixed temperature boundary conditions and use adiabatic and non-adiabatic formulations of the combustion model. The results are compared against the previous fully adiabatic case and experimental data. The statistics for the simulations are similar to the results obtained from the fully adiabatic case. Improved statistics are obtained for the temperature in the near-wall regions. The non-adiabatic flamelet case shows the average reaction rate values at the flame root case are approximately 50 % smaller in comparison to the adiabatic flamelet cases. This causes the lift-off height to be overestimated. Further investigation will be undertaken with the non-adiabatic flamelet case, as the flame is observed to be highly unstable.

Introduction

Lean combustion is utilised in modern gas turbine combustors, in order to reduce the production of pollutants. The stability of lean flames is enhanced through the use of swirling flow, since an Inner Recirculation Zone (IRZ) is formed by the flow field and hot combustion products and radical species are continuously supplied to the flame root to aid flame stabilisation [1]. However, it is well known that lean combustion is highly unstable and such flames are susceptible to local extinction and flame blow-off. The mechanisms leading to blow-off are not well understood and under such conditions, the flame heat release becomes weaker and the heat loss effects can play a more influential role. There has been a number of recent modelling studies on flame blow-off, e.g., Refs. [2, 3], but heat loss effects are seldom considered. Thus, it is of interest from a modelling perspective to observe how heat loss effects can influence the flame behaviour close to lean blow-off conditions.

Large Eddy Simulation (LES) has proven to be successful at modelling heat loss effects in simulations of turbulent flames. One approach for including heat loss effects is to account for heat transfer from the walls of the combustion chamber, which can lead to achieving improved accuracy. A simple approach is by imposing wall temperature boundary conditions (for example [4] and therein). Alternative methods include a conjugate heat transfer approach [5], or using a fully coupled LES/heat conduction approach, where an additional solver is used to compute the temperature distribution for the solid structure of the combustion chamber [6].

Alternatively, heat loss effects can be modelled by considering non-adiabatic chemistry in flamelet calculations. An early approach considered an enthalpy defect approach in the flamelets [7–9], which is achieved by considering the heat loss through radiation. A burner-stabilised flame method for building the library for the Flamelet Generated Manifold

(FGM) approach was introduced by van Oijen and de Goey [10] and Fiorina et al. [11], where the non-adiabatic effects are obtained by submitting a heat flux to the wall of the burner to decrease the enthalpy in that region. Other approaches have more recently been proposed for non-adiabatic flamelet approaches, which include a wall heat transfer model [12] and a Perfectly Stirred Reactor (PSR) approach for Moderate or Intense Low-oxygen Dilution (MILD) combustion [13]. A final approach is to add a heat sink term on to the heat release term in the energy equation to mimic the heat loss effects across the flame, as proposed in [14, 15].

The gas turbine model combustor developed by the German Aerospace Centre (DLR) is a partially premixed system containing two swirl generators [16, 17]. Extensive measurements using laser diagnostics for three operating conditions were made, which were for thermo-acoustically stable and unstable conditions, and for a flame close to blow-off. The third case is of interest for this study and this flame showed sudden lift-off with partial extinction and re-ignition leading to re-anchoring of the flame to the stabilisation point [18]. Understanding the mechanisms leading to blow-off is challenging, owing to the complex interactions between turbulence, the heat release from combustion and molecular transport [19]. In addition, the study by Palies et al. [20] suggested the use of adiabatic walls can cause significant changes to the shape of the flame and hence, the flame to be studied here may be sensitive to changes when including heat loss effects in the modelling approach. Furthermore, the role of heat loss on the blow-off behaviour of the flame is not clear.

The aim of this work is to investigate the influences of heat loss on the stabilisation of a flame close to blow-off in the gas turbine model combustor. The objectives are to compare two simulations using non-adiabatic wall conditions, where one will also use a non-adiabatic flamelet approach. These results will be compared to the fully adiabatic case that has been studied by Massey et al. [21]. The remainder of this paper is organised as follows. A description of the numerical modelling strategy is outlined next, followed by a description of the gas turbine model combustor experiment to be simulated. The results and observations are presented and the key findings are then shown. The conclusions and key findings of the study are then summarised.

Numerical detail

The numerical approach used for this work is based on the previous study by Chen et al. [22], where an adiabatic flamelet closure was used. This model has been successfully tested for LES studies of premixed and partially premixed combustion in gas turbine systems for both stable and unstable flame simulations [23] for relatively higher global equivalence ratios ($\phi = 0.6$ – 0.8) and thermal powers (10–950 kW). In the present work, heat loss to the chamber walls is considered to be more influential on the flame behaviours under the near blow-off condition ($\phi = 0.55$) with a smaller thermal power of 7.6 kW. Thus, non-adiabatic effects are accounted for at both the LES (through iso-thermal wall boundary condition) and flamelet levels. The individual effects at these two different levels are examined in this study through comparisons with the previous LES results obtained from the fully adiabatic simulation [21]. The details of these three sets of simulations are given in Tab. 1.

Case	AD [21]	NAW	NAF
Fixed temperature BCs	No	Yes	Yes
Non-adiabatic flamelets	No	No	Yes

Table 1: Details of heat loss effects considered in the simulated cases.

Large eddy simulation

The filtered conservation equations for mass and momentum are solved, along with five transport equations for thermochemical variables. These are the total enthalpy (sum of the sensible and chemical enthalpies) h and the filtered mean and variance of the mixture fraction ξ and a normalised reaction progress variable c . These are all obtained from their respective transport equation, which are in the form:

$$\frac{\partial \bar{\rho} \tilde{\varphi}}{\partial t} + \nabla \cdot (\bar{\rho} \tilde{U} \tilde{\varphi}) = \nabla \cdot (\bar{\rho} \tilde{D}_{\text{eff}} \nabla \tilde{\varphi}) + \bar{\mathbf{S}}_{\varphi}^{+} - \bar{\mathbf{S}}_{\varphi}^{-} \quad (1)$$

where \mathcal{D}_{eff} is the effective (laminar + turbulent) diffusivity, where the turbulent part is modelled using the turbulent viscosity μ_T with a turbulent Schmidt number of $\text{Sc}_T = 0.4$ for the ξ and c scalars and a turbulent Prandtl number of $\text{Pr}_T = 0.7$. The vectors of the transported Favre-filtered scalars, sources and sinks are respectively given by

$$\tilde{\varphi} = \left\{ \tilde{\xi}; \sigma_{\xi, \text{sgs}}^2; \tilde{c}; \sigma_{c, \text{sgs}}^2; \tilde{h} \right\}, \quad (2)$$

$$\bar{\mathbf{S}}_{\varphi}^{+} = \left\{ 0; 2 \frac{\mu_T}{\text{Sc}_T} |\nabla \tilde{\xi}|^2; \bar{\omega}^*; 2 \frac{\mu_T}{\text{Sc}_T} |\nabla \tilde{c}|^2 + 2 (\bar{c} \bar{\omega}^* - \tilde{c} \tilde{\omega}^*); 0 \right\}, \quad (3)$$

$$\bar{\mathbf{S}}_{\varphi}^{-} = \{0; 2 \bar{\rho} \tilde{\chi}_{\xi, \text{sgs}}; 0; 2 \bar{\rho} \tilde{\chi}_{c, \text{sgs}}; 0\}. \quad (4)$$

The sub-grid Scalar Dissipation Rate (SDR) terms $\tilde{\chi}_{\xi, \text{sgs}}$ and $\tilde{\chi}_{c, \text{sgs}}$ require modelling. The sub-grid SDR for ξ is modelled using a linear relaxation model $\tilde{\chi}_{\xi, \text{sgs}} = C_{\xi} (\nu_T / \Delta^2) \sigma_{\xi, \text{sgs}}^2$ [24]. The sub-grid SDR for c is modelled using the algebraic expression used in previous studies [22, 23].

The Favre-filtered temperature is obtained using the filtered enthalpy transport equation and is calculated using the mixture-averaged enthalpy of formation $\widetilde{\Delta h}_f^0$ and heat capacity \tilde{c}_p through the approximation: $\tilde{T} = T_0 + (\tilde{h} - \widetilde{\Delta h}_f^0) / \tilde{c}_p$, where $T_0 = 298.15$ K. The mixture density is computed using the state equation, $\bar{\rho} = \bar{p} \bar{M} / \mathfrak{R}^0 \tilde{T}$, where \bar{M} represents the Favre-filtered molecular mass of the mixture and \mathfrak{R}^0 is the universal gas constant. These thermochemical properties (\tilde{c}_p , $\widetilde{\Delta h}_f^0$ and \bar{M}) and the reaction source terms terms in Eqs. (3) and (4), $\bar{\omega}^*$ and $\bar{c} \bar{\omega}^*$ respectively, totalling five variables are tabulated in a look-up table prior to the LES. This table is generated using laminar flame solutions along with a presumed-shape joint Probability Density Function (PDF).

The LES framework described above is used for all three simulations listed in Tab. 1. The same four-dimensional look-up table [21] is used for cases AD and NAW. In case NAW, the wall heat loss effects on the temperature field are included when solving for \tilde{h} through the wall boundary condition in the LES, which is detailed in the next section. In addition to this, the heat loss effects at the flamelet level are considered in the NAF case, where an additional dimension for enthalpy is included in the table to integrate the flamelet solutions under a range of heat loss conditions, which is described next.

Non-adiabatic flamelet closure

The filtered reaction rate closure used for partially premixed combustion here accounts for premixed and non-premixed combustion modes and is expressed as $\bar{\omega}^* = \bar{\omega}_{\text{fp}} + \bar{\omega}_{\text{np}}$ [22]. The non-premixed contribution $\bar{\omega}_{\text{np}}$ is significant only in the vicinity of stoichiometric mixture fraction, which is located far from the combustion chamber walls as found in the experiments [17]. Thus, this term is taken to be unaffected by the wall heat losses.

For the premixed mode contribution, the non-adiabatic effects are included following an approach outlined in [14]. In this approach, heat loss is introduced in the one-dimensional freely propagating premixed laminar flame calculations by altering the heat

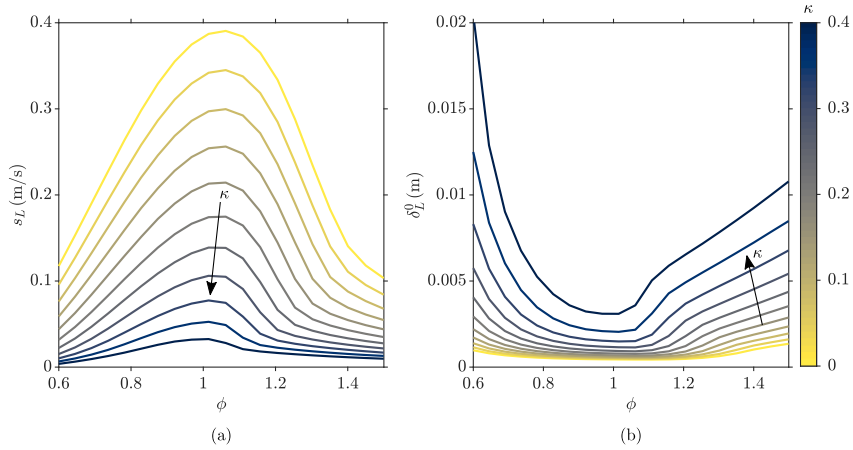


Figure 1: Flamelets generated using the heat release damping approach [14, 15]. The flame speed (a) and flame thickness (b) are plotted against ϕ for different values of κ in the range $0 \leq \kappa \leq 0.4$.

release source term in the energy equation. This equation is implemented in Cantera and in common notations it reads [25]

$$\rho c_p U \frac{dT}{dx} = \frac{d}{dx} \left(\lambda \frac{dT}{dx} \right) + \rho \frac{dT}{dx} \left(\sum_{\alpha=1}^N c_{p,\alpha} \mathcal{D}_\alpha \frac{dY_\alpha}{dx} \right) - (1 - \kappa) \sum_{\alpha=1}^N h_\alpha \dot{\omega}_\alpha, \quad (5)$$

where κ is the introduced heat loss factor. For a given equivalence ratio, laminar flame calculations are performed for a number of κ values ranging from 0 (i.e., adiabatic) to 0.4. These calculations are then repeated for 20 different equivalence ratios covering the flammability range. Note that beyond $\kappa = 0.4$ no flame solution could be obtained for the case near the lean flammability limit. The laminar flamelets are calculated using the GRI Mech 3.0 chemical mechanism and the results for the flame speed s_L and flame thickness δ_L^0 are shown in figures 1a and 1b respectively. The value of κ is progressively decreased from 0 to 0.4 by steps of 0.04 resulting in 11 flamelet solutions for each equivalence ratio. As the heat loss factor increases, the flame speed decreases and the flame thickness increases, as expected. For the highest heat loss case with $\kappa = 0.4$, the value for s_L is less than 5% of the adiabatic value for all equivalence ratios. Therefore, the flame is considered to be quenched for higher heat losses. However, it is possible in the LES that the heat loss (enthalpy defect) is higher than that for $\kappa = 0.4$ at a given local equivalence ratio. To cover this in the flamelet table, four more heat loss levels are included and these solutions are obtained by progressively lowering the gas temperature to 300 K for each solution point in the 1D laminar flame for $\kappa = 0.4$. As a result, only the temperature related quantities (T , c_p , ρ and h) are different in these four additional solutions, whereas the mixture composition remains the same as that for $\kappa = 0.4$. Therefore, in total 15 (heat loss levels) \times 20 (equivalence ratios) flamelet solutions are computed using Cantera, and subsequently, these 1D solutions are interpolated into 3D space and parameterised by the mixture fraction, progress variable and enthalpy.

The mixture fraction is defined using Bilger's formula. A normalised progress variable using the sum of CO and CO₂ mass fractions is adopted from previous studies [21, 23]. For non-adiabatic flamelets, this definition is extended as

$$c = \frac{Y_{\text{CO}} + Y_{\text{CO}_2}}{Y_{\text{CO}}^b(\xi, h^*) + Y_{\text{CO}_2}^b(\xi, h^*)}, \quad (6)$$

where the superscript ^b denotes the flame burnt side value and the normalised enthalpy

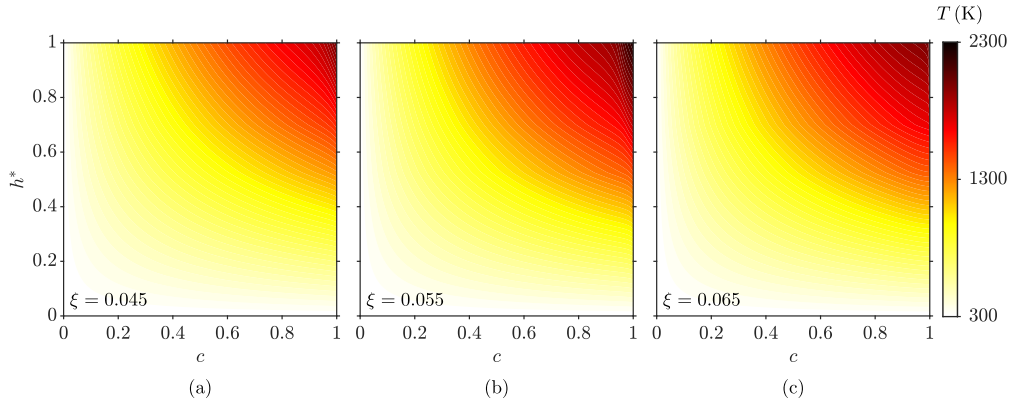


Figure 2: Contour plots of the flamelet temperature over progress variable c and normalised enthalpy h^* space.

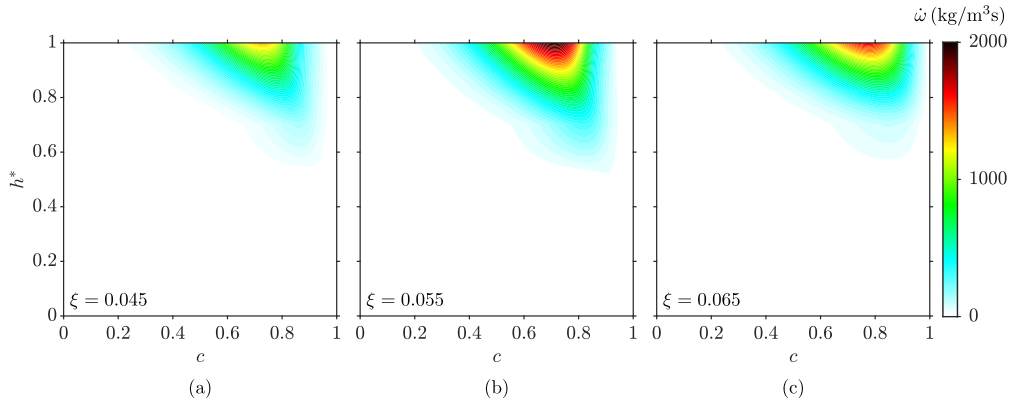


Figure 3: Contour plots of the flamelet reaction rate over progress variable c and normalised enthalpy h^* space.

is given by

$$h^* = \frac{h - h^{\min}(\xi, c)}{h^{\text{ad}}(\xi, c) - h^{\min}(\xi, c)}, \quad (7)$$

where the superscripts \min and ad denote the minimum and adiabatic mixture enthalpies respectively for the given ξ and c . The values of h^{\min} and h^{ad} are tabulated as functions of ξ and c for the normalisation of filtered enthalpy in the LES. Figures 2 and 3 show the temperature and progress variable reaction rate fields obtained from the flamelet calculations in c and h^* space for three representative ξ values. It can be seen that the reaction rate is zero when $h^* < 0.6$ for all three mixture fractions, whereas the temperature smoothly decreases to 300 K as h approaches zero. This is physically consistent with the heat loss process when the flame is quenched by the wall and the reaction rate drops to zero but the temperature decreases gradually through the heat conduction.

These laminar flame solutions are then used for the integration of filtered quantities required in the LES. Following the previous study [13], the filtered premixed reaction rate source term is modelled as

$$\bar{\dot{\omega}}_{\text{fp}} = \bar{\rho} \int_0^1 \int_0^1 \int_0^1 \frac{\dot{\omega}(\eta, \zeta, \theta)}{\rho(\eta, \zeta, \theta)} \tilde{P}(\eta, \zeta, \theta) \, \text{d}\eta \, \text{d}\zeta \, \text{d}\theta, \quad (8)$$

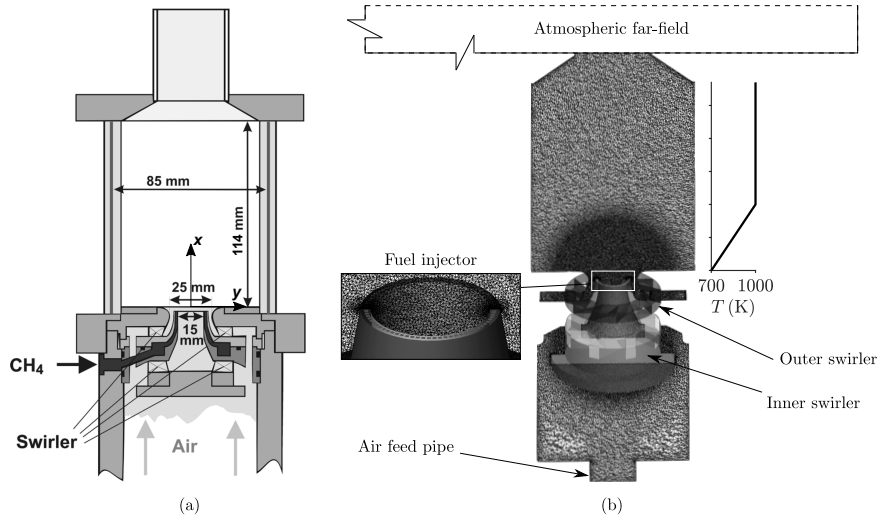


Figure 4: Schematic drawing of the gas turbine model combustor [16, 17].

where

$$\tilde{P}(\eta, \zeta, \theta) \approx \tilde{P}_\beta(\eta; \tilde{\xi}, \sigma_{\xi, \text{sgs}}^2) \times \tilde{P}_\beta(\zeta; \tilde{c}, \sigma_{c, \text{sgs}}^2) \times \delta(\theta - \tilde{h}^*) \quad (9)$$

is the joint PDF of mixture fraction, progress variable and normalised enthalpy with η , ζ and θ being their sample space variables respectively. The presumed β -distribution is used for ξ and c , while a Dirac δ -function is used for h^* . The other source term $c\tilde{\omega}^*$ is calculated in a manner similar to $\bar{\omega}_{\text{fp}}$. The other source term $\bar{c}\tilde{\omega}^*$ and the filtered thermochemical variables, $\widetilde{\Delta h}_f^0$, \tilde{c}_p and \tilde{M} , are calculated in a manner similar to $\bar{\omega}_{\text{fp}}$ in Eq. (8).

Gas turbine model combustor

Test case

A schematic of the DLR combustor is shown in Fig. 4a; a full description of the measurement techniques are outlined in [16–18]. The combustion chamber had a square cross-section of internal area of $85 \times 85 \text{ mm}^2$ and a length of 114 mm. Dry air at atmospheric pressure and room temperature entered a single plenum and then passed through two radial swirlers. The two co-swirling flows entered the combustion chamber through a central nozzle of diameter 15 mm and an annular nozzle with inner and outer diameters of 17 mm and 25 mm respectively. Methane was fed through a non-swirling nozzle ring having 72 channels ($0.5 \times 0.5 \text{ mm}^2$) located between the two air nozzles. The exit planes of the central air and methane nozzles are 4.5 mm below the exit of the annular air nozzle and the entrance to the combustion chamber. The flow rates for air and methane for the flame close to blow-off, referred to as flame C, are listed in Tab. 2 along with the thermal power and global equivalence ratio. Under these operating conditions, the flame root was positioned at an average height of approximately 6 mm above the fuel nozzle. The flame was observed to be highly unstable with random sudden lift-off events and the flame base returning to the location $x = 1.5 \text{ mm}$. These lift-off events typically lasted 0.1–0.15 s and occurred 1–2 times per second. The stabilised flame and its lift-off events were shown by [18] using the time sequences of the combined high-speed (5 kHz) PIV and OH-PLIF images.

Computational model and solver

The computational domain is shown in Fig. 4b, which consists of 20 million unstructured tetrahedral cells. This includes an air feed pipe, the plenum, both swirlers, the combustor,

Parameter	Value	Description
\dot{m}_{air}	4.68 g/s	Air flow rate through the plenum
\dot{m}_{CH_4}	0.15 g/s	Methane flow rate through the nozzle
P_{th}	7.6 kW	Overall thermal power
S	0.55	Swirl number
ϕ_{glob}	0.55	Global equivalence ratio

Table 2: Operating conditions for flame C [16, 17].

tion chamber and a large cylindrical atmospheric far-field downstream of the combustion chamber exit, in order to prevent acoustic wave reflection. All of the walls have no-slip conditions imposed, apart from the walls in the streamwise direction of the extended far-field domain, which have slip conditions imposed. The bottom plane of the combustion chamber is given an isothermal boundary condition of 700 K and the side walls of the combustion chamber have a linear profile up to 40 mm that increases from 700 K to 1000 K; beyond 40 mm, the side walls are at 1000 K. The outlet is specified to have zero streamwise gradients for all the variables. The air feed pipe and fuel injector have constant mass flow rate boundary conditions imposed using the values in Tab. 2 along with a top-hat velocity profile. All 72 fuel injectors are included in the mesh to provide an improved accuracy for the fuel-air mixing.

The simulations are performed using OpenFOAM 2.3.0 and the PIMPLE algorithm is used for pressure-velocity coupling. Second-order central difference schemes are used for the spatial derivatives and a first-order implicit Euler scheme is used for the temporal derivatives. Therefore, a small time step of $\Delta t = 0.15 \mu\text{s}$ is used to ensure suitable accuracy for the time derivatives and that the CFL number remains below 0.4 across the whole domain. The simulations were ran on ARCHER, a national high performance computing facility in the United Kingdom. The cases AD, NAW and NAF require around 80, 100, 60 respectively of physical time to allow initial transients to pass out of the domain. The time-averaged statistics are computed using samples collected over 24 ms after the initial transient periods. This 24 ms sample corresponds to roughly 6 flow-through times.

Results

Figure 5 shows typical time-averaged statistics comparisons between the three simulations and measurements for the Favre-filtered axial velocity at different heights from the exit of the annular nozzle. The axial velocity and mixture fraction profiles are shown in Figs. 5a and 5b respectively. It is seen in Fig. 5a that all three simulations show the same variation in the near-field, with some under prediction in the peak axial velocity at $x = 5$ and $x = 10$ mm. Further downstream, cases AD and NAW show the same trend, whereas there is a small shift of the peaks away from the centreline for case NAF. This suggests that when the heat loss effects are included in the canonical model, i.e., premixed flamelets, the opening angle of the swirl flame becomes slightly larger due to weakened reaction rates in the inner shear layer, which is shown later in this section. The results at $x = 20$ and $x = 30$ mm suggest that the width of the IRZ at this location is over predicted for all three cases. However, the velocity variation is captured well at $x = 60$ mm in the LES showing very good agreement with the measurements. For the mixture fraction, by contrast, all three simulations give quite similar predictions at all axial positions in Fig. 5b, suggesting that the overall mixing field is captured well in the LES regardless of the heat loss modelling. All three cases marginally over predict the mixture fraction at all streamwise locations. On the whole, the change in conditions for the three cases does

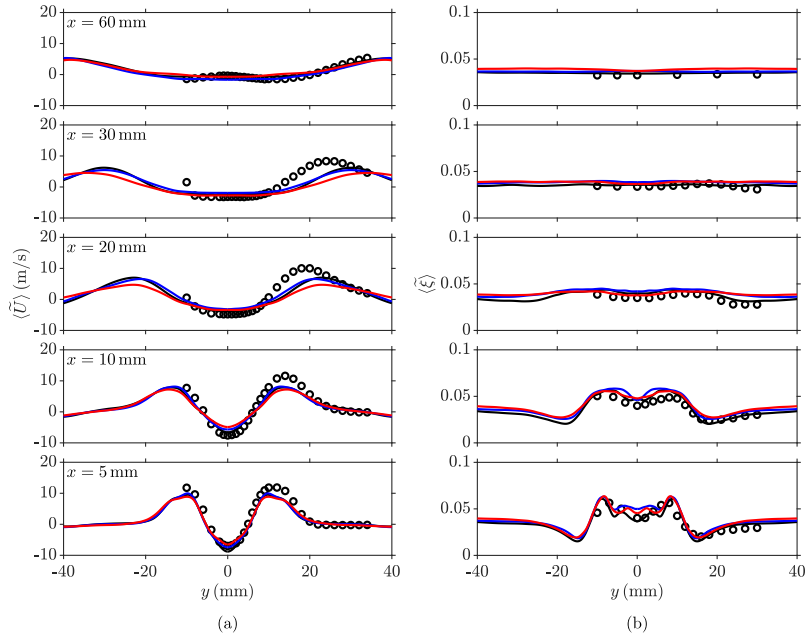


Figure 5: Comparisons of the time-averaged (a) axial velocity and (b) mixture fraction between the measurements [16, 17] (symbols) and the computations (lines), where the latter results are azimuthally averaged. The computations are cases AD (—), NAW (—) and NAF (—).

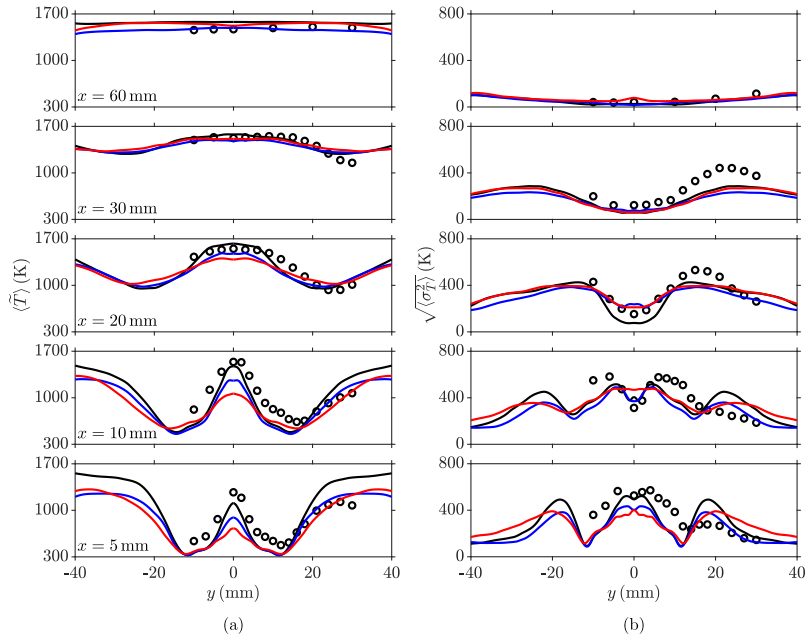


Figure 6: Comparisons of the time-averaged (a) mean and (b) rms temperature between the measurements [16, 17] (symbols) and the computations (lines), where the latter results are azimuthally averaged. The computations are cases AD (—), NAW (—) and NAF (—).

not affect the axial velocity and mixture fraction fields.

The computed and measured temperature profiles are compared in Figs. 6a and 6b for the mean and resolved rms values respectively. For the near-field positions $x = 5$ and 10 mm in Fig. 6a, the mean temperature is over predicted by 20–30% in case AD for large radial positions ($|y| > 20$ mm) when moving towards the wall, where adiabatic wall

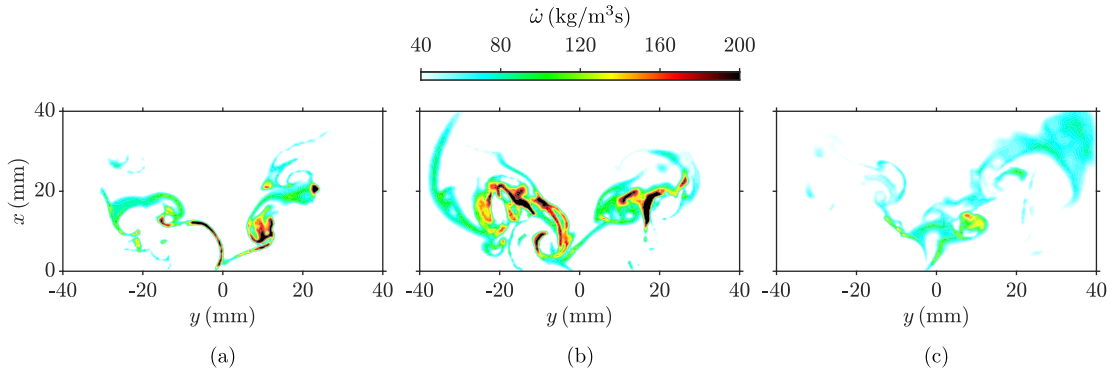


Figure 7: Filtered reaction rate fields for cases AD (a), NAW (b) and NAF (c) on the y - z mid-plane.

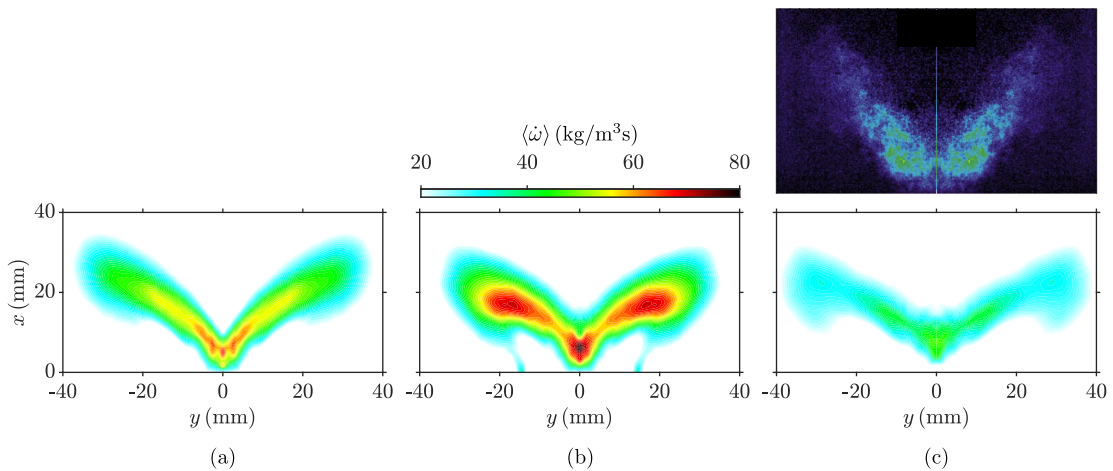


Figure 8: Time and azimuthally-averaged filtered reaction rate fields for cases AD (a), NAW (b) and NAF (c) on the y - z mid-plane. The image above is the averaged CH-LIF image [17].

boundary condition are imposed. The over predictions of the near-wall temperature for case AD are also seen in the rms temperature profiles in Fig. 6b. By contrast, the predictions given by NAW and NAF improve significantly in this region showing good agreement with the experimental data. This suggests that the temperature profiles specified on the combustion dump plane and side wall are satisfactory. The temperature at $x = 5$ mm and 10 mm along the centreline is under predicted by 13% and 4% respectively for case AD. However, significant decreases are seen in the centreline temperature at these two locations for cases NAW and NAF, due to the presence of non-adiabatic effects. This can also be seen in the rms profiles for cases NAW and NAF, as shown in Fig. 6b. This under prediction of centreline temperature in the non-adiabatic cases NAW and NAF indicates an over predicted flame lift-off height. In addition, the temperature in the jet regions in the near-field at $x = 5$ mm are under predicted for all three cases. Therefore, the effect of non-adiabatic conditions severely affects the flame root and its position, which dictate the overall stability and eventual blow-off behaviours of this flame, as observed in [18, 21]. In the regions further downstream from $x = 20$ mm, the profiles for all three cases are similar and hence, the non-adiabatic modelling only significantly affects the flame in the near-field, as also found in a recent LES study [4].

Instantaneous snapshots of the filtered reaction rate of the progress variable for the three LES cases are shown in Fig. 7. It is shown in Fig. 7a that the flame appears to be thinner and more stable for case AD, whereas the reactions are distributed over a

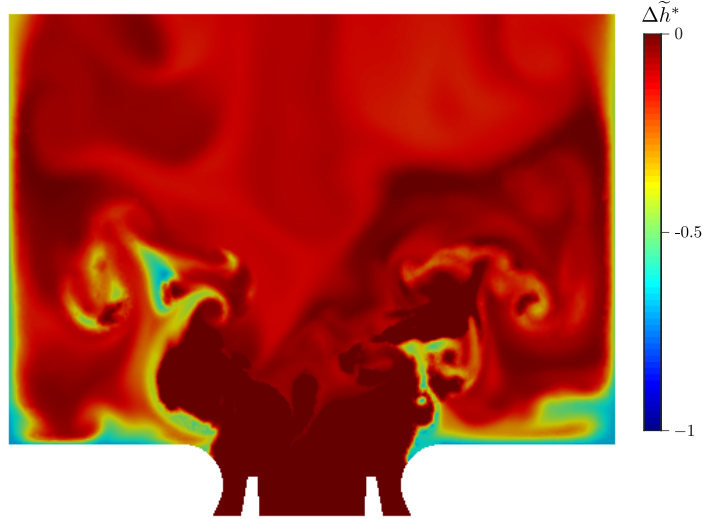


Figure 9: Filtered normalised enthalpy deficit $\Delta\tilde{h}^*$ distribution on the y - z mid-plane for case NAF.

larger region for case NAW in Fig. 7b. In addition, the flames for these two cases have an established flame root with high values for the filtered reaction rate. Both of these observations are seen in the time-averaged fields in Fig. 8. The reaction rate values are higher in case NAW in comparison to case AD because the local mixture fractions for case NAW are slightly higher and closer to stoichiometry, specifically in the regions further away from the centreline at $|y| \approx 20$ mm (see Fig. 5b). However, the averaged field for case NAW shows that the flame stabilises on the wall of the annular air nozzle and a different flame shape is shown compared to the other two cases. This behaviour must be highly avoided because it provides an additional but unphysical anchoring point for the flame and thus, the conditions used in the modelling approach cannot be used for further investigation on flame blow-off behaviours, despite the improvements obtained for the temperature in the near-wall regions.

The instantaneous and time-averaged filtered reaction rates for case NAF, as seen in Figs. 7c and 8c, show that there is a significant decrease in the local values for the reaction rate, which is caused by including the heat loss effects on flamelet reaction rate in the canonical model, as shown earlier in Fig. 3. The average reaction rate values at the flame root for this case are approximately 50% smaller than the values for the adiabatic flamelet cases, as well as along the inner shear layer. The time-averaged contour also shows that the flame root is in a higher position in comparison to cases AD and NAW. The normalised filtered enthalpy deficit $\Delta\tilde{h}^* = \tilde{h}^* - 1$ for the same instantaneous snapshot in Fig. 9 shows that the enthalpy drop is approximately 10% near the flame root, which corresponds to a decrease in the average reaction rate by approximately 25%. Regions of a higher enthalpy decrease around the flame's average position further downstream (as marked in Fig. 8c) and including the heat loss does cause the flame opening angle to increase, as noted previously. The angle is highest for this case compared to the other cases and the CH-LIF image in Fig. 8. It has been observed in a time sequence (not shown here) that the flame root's position varied considerably more than in case AD, and this is closer to the experimental observations [18] showing drastic movement and frequent disappearance of the flame root. Hence, case NAF is of interest for further investigation on the ultimate blow-off of the flame in a future study.

Conclusions

A flame close to blow-off in a dual swirl gas turbine combustor has been investigated using different techniques to model heat loss and compared against a fully adiabatic simulation, referred to as case AD. The combustion model is based on unstrained flamelets with a presumed joint PDF approach based on the mixture fraction, progress variable and the normalised enthalpy, where the latter is included in the PDF to introduce the heat loss effects. Two simulations are studied using fixed wall temperature boundary conditions with and without heat loss, referred to as cases NAF and NAW respectively, in the combustion model and the cases are compared against the baseline adiabatic simulation and experimental data. The axial velocity and mixture fraction statistics are unaffected by the non-adiabatic effects, but some differences are seen for the temperature statistics. Cases NAW and NAF yield improved comparisons between the temperature and the experiment for the near-wall regions, as case AD considerably over predicted the temperature in those regions. However, a change in flame shape is seen for case NAW, as the flame is anchored to the walls of the annular nozzle, which would change the blow-off behaviour of the flame. In addition, cases NAW and NAF show under predictions the average centreline temperature at the near-field and indicate that the flame root height is over predicted. Given the highly unstable behaviour of the non-adiabatic flamelet case, it is of interest to investigate this case further.

Acknowledgements

J. C. Massey acknowledges the financial support from the EPSRC provided through a doctoral training award. The additional support from Rolls Royce plc. is also acknowledged. Z. X. Chen and N. Swaminathan acknowledge the financial support from Mitsubishi Heavy Industries, Ltd., Japan. This work used the ARCHER UK National Supercomputing Service (<https://www.archer.ac.uk>) with the resources provided by the UKCTRF.

Selected references

- [1] Syred, N., “A review of oscillation mechanisms and the role of the precessing vortex core (PVC) in swirl combustion systems”, *Prog. Energy Combust. Sci.* 32(2): 93–161 (2006).
- [2] Zhang, H., Mastorakos, E., “Prediction of Global Extinction Conditions and Dynamics in Swirling Non-premixed Flames Using LES/CMC Modelling”, *Flow, Turbul. Combust.* 96(4): 863–889 (2016).
- [3] Ma, P.C., Wu, H., Labahn, J.W., Jaravel, T., Ihme, M., “Analysis of transient blow-out dynamics in a swirl-stabilized combustor using large-eddy simulations”, *Proc. Combust. Inst.* 37(4): 5073–5082 (2019).
- [4] Benard, P., Lartigue, G., Moureau, V., Mercier, R., “Large-Eddy Simulation of the lean-premixed PRECCINSTA burner with wall heat loss”, *Proc. Combust. Inst.* 37(4): 5233–5243 (2019).
- [5] Bauerheim, M., Staffelbach, G., Worth, N.A., Dawson, J.R., Gicquel, L.Y.M., Poinot, T., “Sensitivity of LES-based harmonic flame response model for turbulent swirled flames and impact on the stability of azimuthal modes”, *Proc. Combust. Inst.* 35(3): 3355–3363 (2015).
- [6] Kraus, C., Selle, L., Poinot, T., “Coupling heat transfer and large eddy simulation for combustion instability prediction in a swirl burner”, *Combust. Flame* 191: 239–251 (2018).
- [7] Bray, K.N.C., Peters, N., “Laminar flamelets in turbulent flames”, in *Turbulent Re-*

- acting Flows*, edited by P.A. Libby, F.A. Williams, chap. 2, pp. 63–113, Academic Press, London, UK (1994).
- [8] Marracino, B., Lentini, D., “Radiation modelling in non-luminous nonpremixed turbulent flames”, *Combust. Sci. Technol.* 128(1–6): 23–48 (1997).
 - [9] Hossain, M., Jones, J.C., Malalasekera, W., “Modelling of a bluff-body nonpremixed flame using a coupled radiation/flamelet combustion model”, *Flow, Turbul. Combust.* 67(3): 217–234 (2002).
 - [10] van Oijen, J.A., de Goey, L.P.H., “Modelling of Premixed Laminar Flames using Flamelet-Generated Manifolds”, *Combust. Sci. Technol.* 161(1): 113–137 (2000).
 - [11] Fiorina, B., Baron, R., Gicquel, O., Thevenin, D., Carpentier, S., Darabiha, N., “Modelling non-adiabatic partially premixed flames using flame-prolongation of ILDM”, *Combust. Theory Model.* 7(3): 449–470 (2003).
 - [12] Ma, P.C., Wu, H., Ihme, M., Hickey, J.P., “Nonadiabatic Flamelet Formulation for Predicting Wall Heat Transfer in Rocket Engines”, *AIAA J.* 56(6): 2336–2349 (2018).
 - [13] Chen, Z.X., Doan, N.A.K., Lv, X.J., Swaminathan, N., Ceriello, G., Sorrentino, G., Cavaliere, A., “Numerical Study of a Cyclonic Combustor under Moderate or Intense Low-Oxygen Dilution Conditions Using Non-adiabatic Tabulated Chemistry”, *Energy and Fuels* 32(10): 10256–10265 (2018).
 - [14] Proch, F., Kempf, A.M., “Modeling heat loss effects in the large eddy simulation of a model gas turbine combustor with premixed flamelet generated manifolds”, *Proc. Combust. Inst.* 35(3): 3337–3345 (2015).
 - [15] Wollny, P., Rogg, B., Kempf, A., “Modelling heat loss effects in high temperature oxy-fuel flames with an efficient and robust non-premixed flamelet approach”, *Fuel* 216: 44–52 (2018).
 - [16] Meier, W., Duan, X.R., Weigand, P., “Investigations of swirl flames in a gas turbine model combustor: II. Turbulence-chemistry interactions”, *Combust. Flame* 144(1–2): 225–236 (2006).
 - [17] Weigand, P., Meier, W., Duan, X.R., Stricker, W., Aigner, M., “Investigations of swirl flames in a gas turbine model combustor: I. Flow field, structures, temperature, and species distributions”, *Combust. Flame* 144(1–2): 205–224 (2006).
 - [18] Stöhr, M., Boxx, I., Carter, C., Meier, W., “Dynamics of lean blowout of a swirl-stabilized flame in a gas turbine model combustor”, *Proc. Combust. Inst.* 33(2): 2953–2960 (2011).
 - [19] Shanbhogue, S.J., Husain, S., Lieuwen, T.C., “Lean blowoff of bluff body stabilized flames: Scaling and dynamics”, *Prog. Energy Combust. Sci.* 35(1): 98–120 (2009).
 - [20] Palies, P., Schuller, T., Durox, D., Gicquel, L.Y.M., Candel, S., “Acoustically perturbed turbulent premixed swirling flames”, *Phys. Fluids* 23: 037101 (2011).
 - [21] Massey, J.C., Chen, Z.X., Swaminathan, N., “Lean Flame Root Dynamics in a Gas Turbine Model Combustor”, *Combust. Sci. Technol.* (Submitted) (2018).
 - [22] Chen, Z., Ruan, S., Swaminathan, N., “Large Eddy Simulation of flame edge evolution in a spark-ignited methane-air jet”, *Proc. Combust. Inst.* 36(2): 1645–1652 (2017).
 - [23] Chen, Z.X., Swaminathan, N., Stöhr, M., Meier, W., “Interaction between self-excited oscillations and fuel-air mixing in a dual swirl combustor”, *Proc. Combust. Inst.* 37(2): 2325–2333 (2019).
 - [24] Pitsch, H., “Large-Eddy Simulation of Turbulent Combustion”, *Annu. Rev. Fluid Mech.* 38(1): 453–482 (2006).
 - [25] Goodwin, D.G., Moffat, H.K., Speth, R.L., “Cantera: An Object-oriented Software Toolkit for Chemical Kinetics, Thermodynamics, and Transport Processes”, (2017).